Formation of a Unique Crystal Morphology for the Poly(ethylene glycol)−Poly(ϵ-caprolactone) Diblock Copolymer

Chaoliang He, Jingru Sun, Ting Zhao, Zhongkui Hong, Xiuli Zhuang, Xuesi Chen,* and Xiabin Jing

State Key Laboratory of Polymer Physics and Chemistry, Changchun Institute of Applied Chemistry, Graduate School of Chinese Academy of Sciences, Chinese Academy of Sciences, Changchun 130022, P. R. China

Received August 30, 2005; Revised Manuscript Received October 17, 2005

The crystallization behaviors of the poly(ethylene glycol)−poly(ϵ-caprolactone) diblock copolymer with the PEG weight fraction of 0.50 (PEG_{50}−PCL_{50}) was studied by DSC, WAXD, SAXS, and FTIR. A superposed melting point at 58.5 °C and a superposed crystallization temperature at 35.4 °C were obtained from the DSC profiles running at 10 °C/min, whereas the temperature-dependent FTIR measurements during cooling from the melt at 0.2 °C/min showed that the PCL crystals formed starting at 48 °C while the PEG crystals started at 45 °C. The PEG and PCL blocks of the copolymer crystallized separately and formed alternating lamella regions according to the WAXD and SAXS results. The crystal growth of the diblock copolymer was observed by polarized optical microscope (POM). An interesting morphology of the concentric spherulites developed through a unique crystallization behavior. The concentric spherulites were analyzed by in situ microbeam FTIR, and it was determined that the morphologies of the inner and outer portions were mainly determined by the PCL and PEG spherulites, respectively. However, the compositions of the inner and outer portions were equal in the analysis by microbeam FTIR.

Introduction

Biodegradable and biocompatible aliphatic polyesters have received great attention over the past two decades. Among them, poly(ϵ-caprolactone) (PCL), poly(lactic acid), poly(glycolic acid), and their copolymers have been widely developed in medical applications, for example, in bone fracture fixation, as sutures, as tissue engineering scaffolds, and as drug release carriers.[1−5] The synthesis of the biomacromolecules above has been extensively developed.[6−12] At the same time, their crystallization behaviors and physical properties have received extensive study as well.[13−20] Recently, poly(ethylene glycol)−poly(ϵ-caprolactone) (PEG−PCL) block copolymers have been developed for their unique properties, such as biocompatibility, amphiphilicity, self-assembly, permeability, and controllable biodegradability.[21] It was established that both the drug permeability and biodegradability relied greatly on the crystallization behaviors of the copolymer.[22] However, because PEG and PCL have comparable crystallization temperatures and glass transition temperatures, the crystallization behaviors of PEG−PCL block copolymer are considerably complicated. Therefore, studies of the crystallization properties and morphology of such block copolymers are rather limited.[23−30] Nojima et al.[23] studied the morphology of the PCL−PEG−PCL triblock copolymers. It was concluded that the PEG and PCL crystals existed independently and there was no eutectic crystal composed of the two blocks. Gan et al.[24,25] studied the isothermal crystallization and melting behavior of the Poly(ethylene oxide) (PEO)−PCL diblock copolymers with a PEO weight fraction of 0.20. Bogdanov et al.[26,27] characterized the thermal properties of PEG−PCL block copolymers of three different structures with PCL weight fractions of 0.68−0.81. It was established that the PCL block crystallized first and fixed the total structure of the spherulites, leading to significant imperfect crystallization of the PEG block. Shiomi et al.[28] observed unique double concentric spherulites such as concentric circles for the PCL−PEG−PCL triblock copolymers with the PCL weight fractions of 0.60 and 0.66. However, the formation mechanism and interior crystallization information of the double concentric spherulites has not been reported yet. Jiang et al.[29] observed the ring-banded spherulite morphology of a double crystalline PEO−PCL diblock copolymer, in which the weight fraction of the PEO was only 0.185.

In our previous work, the crystallization behaviors and morphology of a series of PEG−PCL diblock copolymers was studied.[30] It was concluded that the crystallizability of each block was determined by the relative block length. An interesting morphology, the concentric spherulites, was observed for the PEG_{50}−PCL_{50} diblock copolymer. The morphology of inner and outer portions of the concentric spherulites was similar to those of the PCL and PEG spherulites, respectively, and seemed to be formed by a macrophase separation of two components, which was known to be impossible for the copolymer with limited chain size. Especially, the spherulites formed later grew concentrically from the front of the spherulites formed earlier. The formation of the unique crystal morphology may be related to some special crystallization kinetics and the interesting mutual effects of the two crystalline blocks. In this paper, the formation mechanism of the concentric spherulites was elucidated by POM, and the interior crystallization behaviors of the unique crystal morphology were analyzed in detail by the infrared microscopy.

Experimental Section

Methods. ϵ-Caprolactone (ϵ-CL, Aldrich) was purified by vacuo distillation over CaH_2. Monomethoxy poly(ethylene glycol) (mPEG,

* To whom correspondence should be addressed. Tel: +86-431-5262112. Fax: +86-431-5685653. E-mail: xschen@ciac.jl.cn.

10.1021/bm050627f CCC: $33.50
Published on Web 11/17/2005

Table 1. Molecular Weights and Crystal Growth Rates of the PEG and PCL Homopolymers and the $PEG_{50}-PCL_{50}$ Diblock Copolymer

	M_n				crystal growth rate, G^c (μm/s)			
sample	PEG	PCL[a]	M_n[b]	M_w/M_n[b]	PCL spherulite	PCL crystal within the PEG spherultie	PEG spherulite	PEG crystal within the PCL spherultie
PEG	5000		5000	1.04			65.5	
$PEG_{50}-PCL_{50}$	5000	5090	9810	1.16	0.28	0.15	4.4	15.1
PCL		5100	5900	1.30	0.41			

[a] Evaluated by ^{1}H NMR. [b] Determined by GPC (calibrated with PEG standards). [c] Measured in the isothermal crystallization at 38 °C by POM.

Mn = 5000, Alfa) was dried by an azeotropic distillation with dry toluene. Toluene was dried through refluxing with sodium metal under argon atmosphere.

Polymerization. The $PEG_{50}-PCL_{50}$ diblock copolymers were synthesized by the ring-opening polymerization of ϵ-CL using mPEG as the macroinitiator and $Sn(Oct)_2$ as the catalyst. mPEG, ϵ-CL, and $Sn(Oct)_2$ (0.1% of ϵ-CL in molar ratio) were weighed into an ampere flask with a magnetic bar. Dry toluene was injected into the flask under argon atmosphere. The flask was sealed under dry argon and then immersed in an oil bath at 130 °C with stirring for 72 h. The product was purified by precipitating twice into cold 2-propanol from the chloroform solution and then was dried in vacuo at room temperature for 24 h. The PCL homopolymer was prepared by a similar procedure, except using 2-propanol as the initiator instead of mPEG.

Sample Preparation. The sample for POM observation was prepared by casting 3 drops of 1 wt % chloroform solution of the polymer on a clean cover glass and then airing for 1 day, followed by drying in vacuo at room temperature for 3 days. The sample for microbeam FTIR was prepared similarly, except using a clean single-side polished silicon wafer instead of the cover glass.

Measurements. Proton nuclear magnetic resonance (^{1}H NMR) spectra of the polymers in deuterated chloroform solutions were recorded by a Bruker 300 MHz spectrometer with tetramethylsilane as internal standard. Gel permeation chromatography (GPC) measurements were carried out by a Waters instrument (515 HPLC pump) equipped with a Wyatt interferometer refractometer. GPC columns used chloroform as the eluent at 25 °C, and the molecular weights were calibrated by the poly(ethylene glycol) standards. Differential scanning calorimetry (DSC) was carried out on a DSC-7 (Perkin-Elmer) under nitrogen atmosphere. Measurements during the first heating from −50 to 100 °C and then the first cooling from 100 to −50 °C as well as the second heating from −50 to 100 °C at 10 °C/min were performed. Wide-angle X-ray diffraction (WAXD) was carried out by a Rigaku X-ray diffractometer with a Ni-filtered Cu Kα radiation (λ = 0.1546 nm) at room temperature. The scanning rate was 4 °/min. The selected voltage and current were 40 kV and 200 mA, respectively. Small-angle X-ray scattering (SAXS) was performed by means of a Philips PW1700 equipped with a Kratky small angle scattering camera, a step-scanning device, and a scintillation counter for recording the scattering intensity. Nickel-filtered Cu Kα radiation (λ = 0.154 nm) was supplied by an X-ray generator operated at 45 kV and 40 mA. The samples for SAXS were maintained at 80 °C for 3 min and then cooled to 38 °C at 0.2 °C/min. The scattering intensities were corrected for absorption, background scattering, and incident X-ray fluctuations of the samples. Crystal growth of the copolymer was observed by polarized optical microscope (POM, Leica DMLP) equipped with a hot stage (Linkam) and a video CCD camera. Temperature-dependent FTIR was carried out by the VERTEX 70 instrument with a temperature controlling accessory. The sample solutions were coated on the KBr plate. The spectra were recorded during heating at 1 °C/min and cooling at 0.2 °C/min. The microbeam FTIR was measured by a HYPERION 3000 infrared microscope, equipped with a color video camera and connected with a Bruker IFS 66V/S infrared spectrometer. The background was calibrated by a clean silicon wafer. In situ microbeam FTIR was performed during the isothermal crystallization on a hot stage.

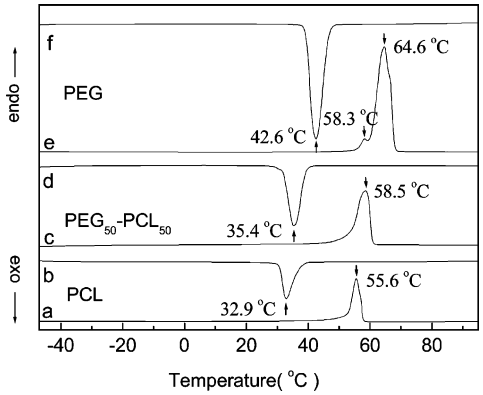

Figure 1. DSC traces of the PEG, PCL, and $PEG_{50}-PCL_{50}$. (a), (c), and (e), second heating. (b), (d), and (f), first cooling. Rate 10 °C/min.

Results and Discussion

Sample Characterization. The PCL weight fraction of the $PEG_{50}-PCL_{50}$ diblock copolymer was calculated by using the relative intensities of the characteristic peak of ^{1}H NMR at 2.28−2.33 ppm for PCL and that at 3.65 ppm for PEG. The molecular weight of the PCL homopolymer was estimated by comparing the intensity of the characteristic peak at 2.28−2.33 ppm for PCL with that at 1.24−1.26 ppm for 2-propanol. The apparent molecular weights and polydispersities of all samples were also measured by GPC. As shown in Table 1, the diblock copolymer exhibited a narrow distribution.

The DSC traces of the PEG, PCL, and $PEG_{50}-PCL_{50}$ are shown in Figure 1. PCL (Mn = 5100) showed single melting and crystallization temperatures at 55.6 and 32.9 °C, respectively. PEG gave two melting points at 64.6 and 58.3 °C and one crystallization temperature at 42.6 °C. The double melting peaks were due to the presence of the PEG crystalline lamellae with different fold numbers.[31] $PEG_{50}-PCL_{50}$ showed the superposed melting and crystallization temperatures at 58.5 and 35.4 °C, respectively.

The crystal structures of all the samples were characterized by WAXD. The PEG and PCL components in $PEG_{50}-PCL_{50}$ exhibited their own diffraction peaks. The WAXD pattern for the diblock copolymer was almost the summation of those for the PEG and PCL homopolymers, suggesting that the PEG and PCL blocks formed separate crystal microdomains.[26,27]

Temperature-dependent FTIR measurements were performed to analyze the slow melting and crystallization process of PEG, PCL, and $PEG_{50}-PCL_{50}$. The crystalline PCL and PEG showed the different characteristic vibrational bands according to respective FTIR spectra of PEG and PCL during the slow melt crystallization. To distinguish clearly the characteristic absorption for the crystallization of each component of $PEG_{50}-PCL_{50}$, the vibrational band at 1196 or 731 cm^{-1} was chosen as the characteristic peak for the crystalline PCL, and the absorption at 843 cm^{-1} for the crystalline PEG. During the heating at 1

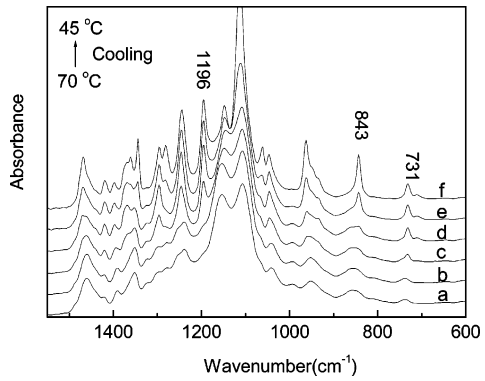

Figure 2. Temperature-dependent FTIR spectra measured during the cooling process for $PEG_{50}-PCL_{50}$. (a) 70 °C. (b) 50 °C. (c) 48 °C. (d) 45 °C, kept for 1 min. (e) 45 °C, kept for 10 min. (f) 45 °C, kept for 20 min. The cooling rate was 0.2 °C/min.

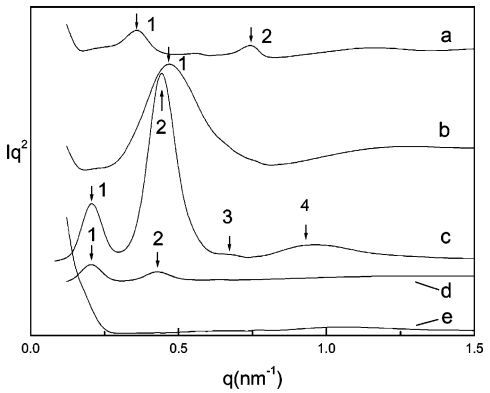

Figure 3. SAXS patterns of PEG (a), PCL (b), and $PEG_{50}-PCL_{50}$ (c, d, e). Curves a, b, and c were measured at 20 °C, curve d was measured at 59 °C, and curve e was measured at 65 °C. The scattering vector $q = (4\pi/\lambda) \sin \theta$.

°C/min, the band for the crystalline PEG (843 cm^{-1}) began to reduce at 55 °C and almost vanished at 58 °C, while that for the crystalline PCL (1196 cm^{-1}) did not begin to decrease until the sample was heated over 59 °C. On the other hand, during the cooling from melt at 0.2 °C/min as shown in Figure 2, the characteristic absorption for the crystalline PCL (1196 cm^{-1}) began to emerge at 48 °C and almost stopped growing at 45 °C, whereas the band for the crystalline PEG (843 cm^{-1}) did not appear until the sample was cooled to 45 °C. Therefore, it could be concluded that the PCL in the copolymer melted later in the heating process and crystallized first in the slow cooling process.

The SAXS results for PEG, PCL, and $PEG_{50}-PCL_{50}$ are shown in Figure 3. Multiple scattering peaks were observed for $PEG_{50}-PCL_{50}$ (curve c). The multiple SAXS peaks for the diblock copolymer suggested that there was a periodic microdomain structure with a long-range order.[32] The four order reflections with the ratios of the q values at the scattering maxima of 1, 2, 3, and 4 in curve c indicated a lamella structure of the diblock copolymer. The long periods of PEG, PCL, and $PEG_{50}-PCL_{50}$ were evaluated from their respective q values at the scattering maximum of the first-order reflection. The long period of the copolymer was 30 nm, and those of PEG and PCL were 18 and 14 nm, respectively. Since there were no eutectic or mixed crystals of the two components, the periodic system of the copolymer should consist of the alternating PCL and PEG domains, with both the crystal lamella and the amorphous layers in each domain. The relatively weak first-order reflection was due to the weak electron density difference between the PCL domain and the PEG domain (341.6 and 354.3 e nm^{-3} for the amorphous PCL and PEG, respectively, at 80 °C, as well as 392.9 and 403.2 e nm^{-3} for the crystalline PCL and PEG, respectively),[23] and the relatively stronger second-order reflection also indicated that the principal scattering arised from the density difference between the crystalline and amorphous layers of each species. The temperature-dependent SAXS measurements were performed to analyze the microdomain structure further. It has been concluded by the temperature-dependent FTIR that the PEG crystals in the copolymer melt first at 55−58 °C while the PCL crystals did not melt until over 59 °C. As shown in Figure 3d, when the sample was heated to about 59 °C, we still observed two scattering peaks with the q values at the scattering maxima equal to the first- and second-order reflections measured at 20 °C, respectively. However, the intensities of both peaks were greatly reduced. The two peaks in curve d corresponded to the first- and second-order reflections for the alternating regions of the PCL crystalline lamellae and the mixture of the amorphous PEG and PCL. Because the PCL crystals formed first during the slow melt crystallization of the copolymer, the PCL crystalline lamellae decided the whole crystal structure of the sample and the melting of PEG crystals did not change the whole periodic distance. The reason the intensities of both peaks reduced was due to the melting of the PEG and partial PCL crystals. After the PCL crystals fully melted at 65 °C, we only observed a very weak correlation hole scattering around 1.1 nm^{-1} in Figure 3e.

POM Observation and Infrared Microscopy Analyses. It is known that the crystallization of macromolecules leads to the birefringent change. To identify the birefringent change clearly, the crystal growth was observed under POM by adding a λ compensator. The real-time micrographs of $PEG_{50}-PCL_{50}$ during the isothermal crystallization at 38 °C are presented in Figure 4, and the POM micrographs of the PEG and PCL homopolymers are shown in Figure 5. The spherulites of PEG, PCL, and $PEG_{50}-PCL_{50}$ were all negative spherulites judged by the characteristic colors of the Maltese cross. Customarily, the quadrants that the vibration direction of the λ compensator located were called quadrants 1 and 3. For the PEG, PCL, and $PEG_{50}-PCL_{50}$ spherulites, quadrants 1 and 3 were close to red (falling color) while quadrants 2 and 4 were close to blue (rising color), indicating a characteristic of the negative spherulites.[33] It suggested that the highest refractive index in the spherulites was tangential and coincided with the chain direction. A unique morphology was developed for $PEG_{50}-PCL_{50}$, as shown in Figure 4. At the beginning, several spherulites such as PCL generated and grew slowly (Figure 4a). When the spherulite radius was plotted against the crystallization time, a linear relationship was obtained (Figure 6a). The growth rate G was approximately 0.28 μm/s. About 177 s later, a sudden birefringent change (became yellow) within a spherulite was observed. The new birefringence diffused extremely quickly within the spherulite and then triggered the growth of a new outer spherulite like PEG from the existing front of the inner spherulite (Figure 4b,c), resulting in the formation of a concentric spherulite. Subsequently, the concentric spherulites generated one after the other. To study the process clearly, the growth process of a concentric spherulite was recorded as shown in Figure 4d−i. Once the preformed single spherulite contacted the front of a neighboring concentric spherulite (Figure 4d), the obvious birefringent change was triggered within the single spherulite. The change process could be described in two steps: first, a brighter sector was formed at the impinging front with the corner toward the single spherulite center, and then,

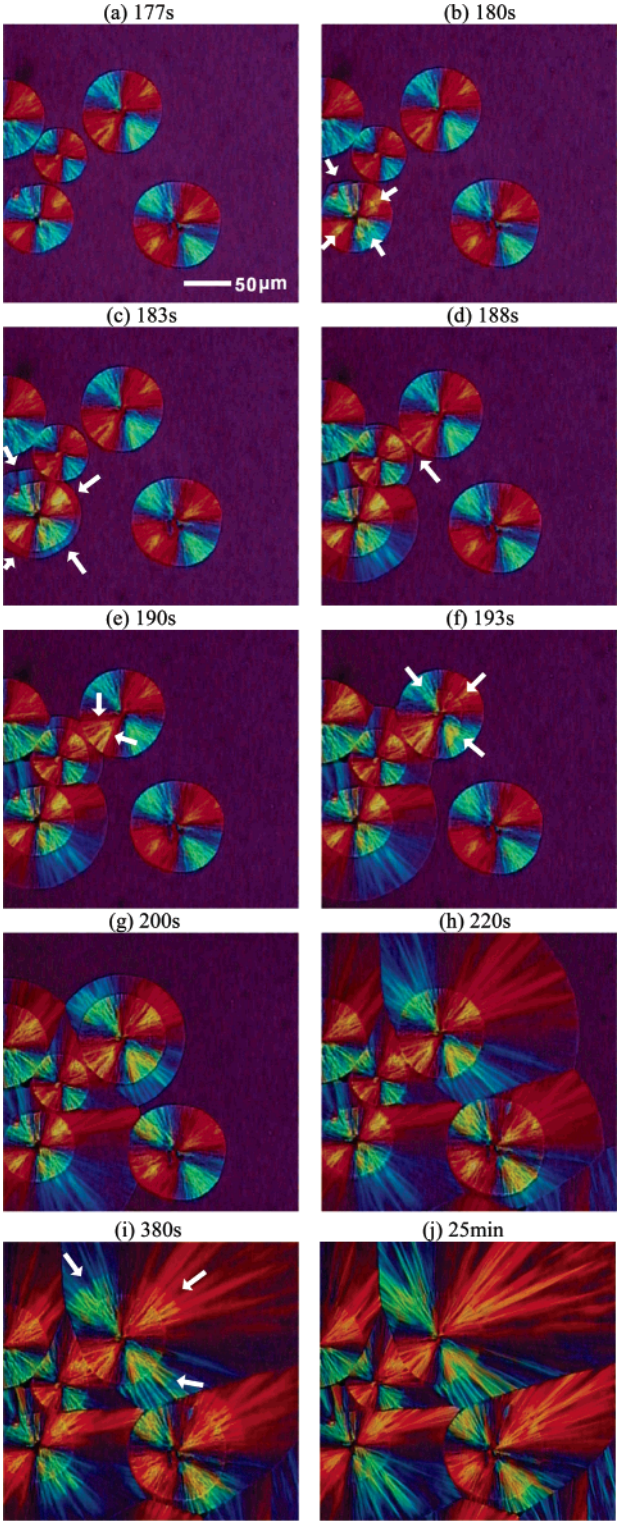

Figure 4. Real-time POM micrographs of PEG_{50}−PCL_{50}. The specimen was melted at 80 °C for 5 min and then quenched to 38 °C at 40 °C/min.

the sector grew larger and larger until its corner reached the spherulite center (Figure 4e); second, once the sector reached the center of the single spherulite, the inward growth was replaced by an outward growth from the single spherulite center (Figure 4f). The growth rate of the new birefringence within the single spherulite was 15.1 μm/s (Figure 6b). Once the new birefringence reached the edge of the single spherulite like PCL, a new outer spherulite like PEG grew concentrically from the existing front of the inner spherulite and formed as the outer

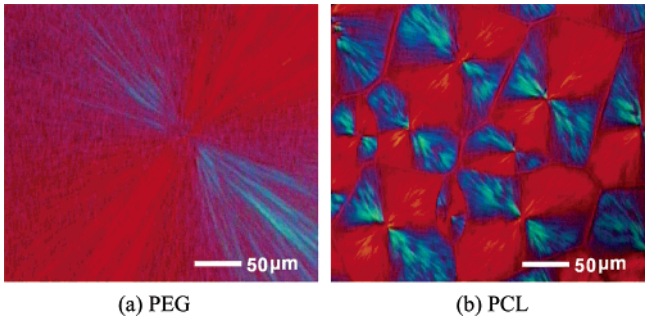

Figure 5. POM micrographs of the PEG (a) and PCL (b) spherulites. The specimen was melted at 80 °C for 5 min and then was quenched to 38 °C at 40 °C/min.

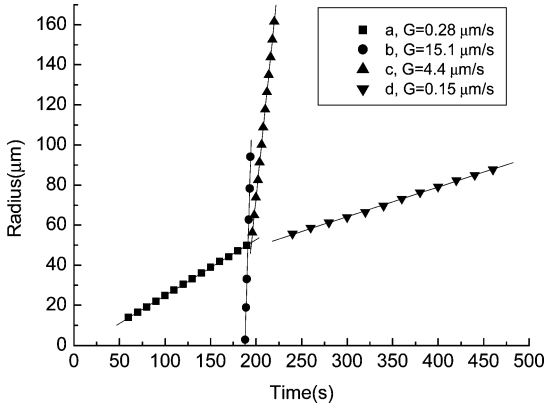

Figure 6. Spherulite radius plotted against the crystallization time at 38 °C for PEG_{50}−PCL_{50}. The slope of the straight line was taken as the radius growth rate *G*. (a) inner PCL spherulite. (b) PEG crystals within the PCL spherulite. (c) outer PEG spherulite. (d) PCL crystals within the outer PEG spherulite.

portion of the concentric spherulite (Figure 4g,h). The growth rate of the outer spherulite was 4.4 μm/s (Figure 6c). Similarly, we also observed the birefringent change within the outer spherulite, following the formation of the concentric spherulite (Figure 4i). The new birefringence pattern seemed to also grow from the front of the inner spherulite, but the morphology of the outer spherulite did not change. The growth rate of the new birefringence within the outer spherulite was 0.15 μm/s (Figure 6d). Finally (25 min later), the whole birefringence was invariable, and the final texture of the concentric spherulites was constructed (Figure 4j).

The whole crystallization process was analyzed by in situ microbeam FTIR. As shown in Figure 7, when the inner spherulite appeared, we only obtained the characteristic absorption for the crystalline PCL (1196 cm^{-1}) in the spherulite (curve 1a), and the exterior part remained in the molten state (curve 2a). Thus, the single spherulite at the moment was the PCL spherulite. About 2 min later, just after the outer spherulite outgrowing from the inner one, the characteristic vibrational bands of both the crystalline PCL (1196 cm^{-1}) and the crystalline PEG (843 cm^{-1}) were observed for the inner spherulite (curve 1b), while only the absorption corresponding to the crystalline PEG (843 cm^{-1}) appeared for the outer spherulite (curve 2b). Therefore, it could be concluded that the quick birefringent change within the inner PCL spherulite was due to the PEG crystallization, and the outer portion of the concentric spherulite was the PEG spherulite. About 25 min later, the vibrational band of the crystalline PCL (1196 cm^{-1}) was observed in the outer spherulite (curve 2c). It suggested that the new slow birefringent change within the outer PEG spherulite was due to the crystallization of the PCL blocks. At

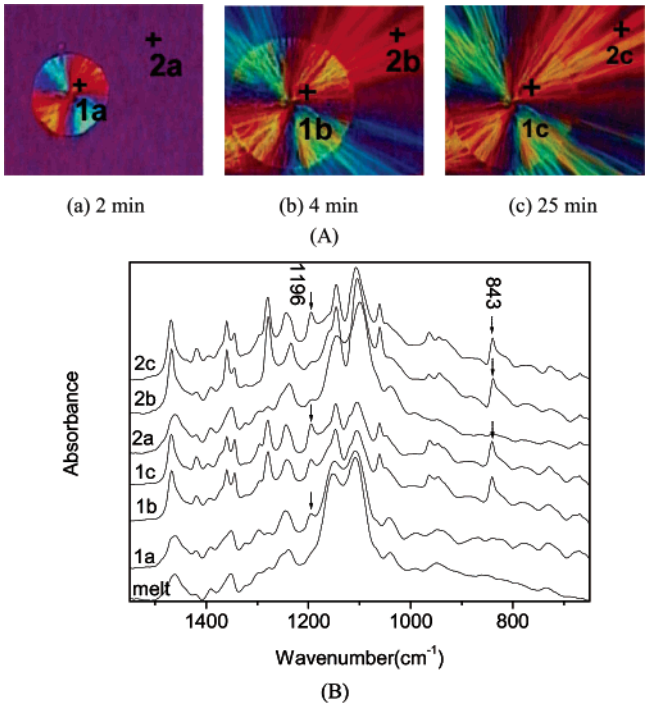

Figure 7. In situ microbeam FTIR spectra measured at the +-marked positions during the isothermal crystallization of $PEG_{50}-PCL_{50}$ at 38 °C. The pictures in (A) show the measured positions and times to take the corresponding spectra (B).

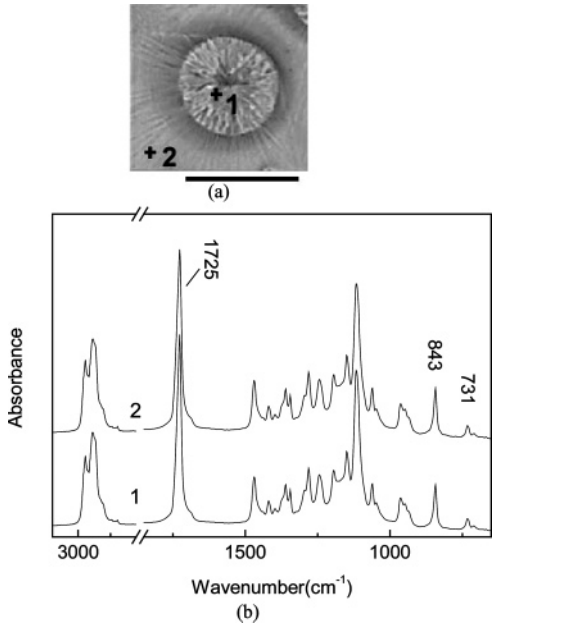

Figure 8. Microbeam FTIR spectra (b) of the $PEG_{50}-PCL_{50}$ concentric spherulites measured at the spots marked by + shown in (a). The sample melt crystallized at 38 °C before being measured. The bar is 100 μm.

the same time, the absorption for the crystalline PCL (1196 cm^{-1}, curve 1c) in the inner spherulite became more intense than ever (curve 1b), due to the further perfection of the PCL crystals of the inner PCL spherulite.

The whole growth process of the concentric spherulites can be explained as follows. At first, the PCL spherulites were nucleated and grew rather slowly. When the PCL blocks were folded into the lamellae of the PCL spherulites, the molten PEG blocks must be sandwiched between the PCL crystalline lamellae. After the induction time, the initial PEG crystal nucleus appeared, which often generated in an existing PCL spherulite (Figure 4b). Since the crystal structures of PCL and PEG were different, direct growth of the PEG crystals on the PCL crystals was difficult. The PEG crystals should be nucleated from the same nuclei (e.g., dusts in the sample) for the PCL spherulites. And only in this case, the outgrown PEG spherulite could be concentric with the inner PCL spherulite as shown in Figure 4b,c. The PEG crystals grew so quickly that it outgrew from the PCL spherulite instantly and kept growing from the existing front of the PCL spherulite. When the marching PEG crystal front appeared at the edge of a neighboring PCL spherulite, the PEG blocks tethered within the interlamellar regions of the PCL spherulite was induced to crystallize, resulting in the inward and then outward growth of the PEG crystals along the radial of the PCL spherulite (Figure 4e,f) because of the symmetrical radial structure of the PCL spherulite within the resolution scale of POM.[34] The growth rate (15.1 μm/s) of the PEG crystals within the interlamellar regions of the inner PCL spherulites was much quicker than that out of the PCL spherulites (4.4 μm/s). The reason might be that the effective concentration of the molten PEG blocks tethered within the interlamellar regions of the inner PCL spherulite was much higher than the average melt concentration. When the outward-growing PEG crystals within the PCL spherulite reached the front of the PCL spherulite, the molten PEG blocks around the PCL spherulite was induced to crystallize in succession and form the outer PEG spherulite (Figure 4g,h). Finally, the molten PCL blocks within the interlamellar regions of the outer PEG spherulite were also induced to crystallize by the crystal front of the inner PCL spherulite (Figure 4i), but the PCL crystallization did not change the total morphology of the outer PEG spherulite. The growth rate of the PCL crystals within the outer PEG spherulite (0.15 μm/s) was obviously slower than that of the inner PCL spherulite (0.28 μm/s). The reason was not clarified by the presently experimental results.

It was established that there was a morphological transition for PEG at 38 ± 2 °C from positive spherulitoids to negative spherulites.[35] Since PEG, PCL, and $PEG_{50}-PCL_{50}$ all grew the negative spherulites at 38 °C in the current study, there should be a transition of the optical property for the PEG spherulites growing at a slightly higher temperature. The spherulite growth at 40 °C for PEG, PCL, and $PEG_{50}-PCL_{50}$ was observed. It was found that PCL still grew the negative spherulites, while PEG grew the spherulites with the mixed optical property, of which the color differences between the four quadrants could not be clearly discerned.[36] Comparatively, $PEG_{50}-PCL_{50}$ still grew the weakly negative concentric spherulites, suggesting that the growth of the concentric spherulites was not affected obviously by the optical property transition of PEG.

The microbeam FTIR measurements were carried out to estimate the compositions and crystallization behaviors of the inner and outer spherulites, respectively. As shown in Figure 8, the FTIR absorption spectra were measured at the spots 1 and 2, locating in the inner and outer portions of the concentric spherulite, respectively. To obtain the crystallization information of each component, the characteristic peak intensities corresponding to both crystals were integrated. Because the integral value of the PCL carbonyl vibrational band (1725 cm^{-1}) was not influenced by the crystallization obviously, it could be used as the internal reference for comparison. The intensity ratios of 731 cm^{-1} to 1725 cm^{-1} for spots 1 and 2 were 0.049 and 0.046, respectively, and those of 843 cm^{-1} to 1725 cm^{-1} for spots 1 and 2 were 0.15 and 0.18, respectively. Therefore, it suggested that the PCL crystallinity in the inner portion of the concentric

spherulite was a little higher than that in the outer portion, while the PEG crystallinity of the outer portion was a little higher than that of the inner portion, owing to the PEG blocks in the inner portion and the PCL blocks in the outer portion crystallizing under the confined conditions. The relative contents of PCL distributing in the inner and the outer sections of the concentric spherulite were also estimated by taking the ratios of the absorption intensity for the carbonyl (1725 cm^{-1}) of PCL to that for C−H vibrational band of the copolymer (2700−3050 cm^{-1}). The ratios for the carbonyl of PCL in the inner and outer portions were both equal to 0.42. Therefore, it could be concluded that the PCL weight fractions distributing in the inner and outer portions of the concentric spherulites were equal.

From the microbeam FTIR analyses, the compositions of the inner and outer portions of the concentric spherulites were almost equal. Therefore, the formation of the inner and outer spherulites was not due to the gradual separation of the PCL and PEG blocks with different block lengths. The reasons for the formation of the unique concentric spherulites were the cooperation of several aspects as follows. First of all, the crystallization temperatures of the PEG and PCL blocks in the diblock copolymer were very close. In the DSC profile, it showed a superposed crystallization temperature for both blocks. Second, the nucleation of PCL crystals was easier than that of PEG crystals. Third, the growth rate of the PEG crystals was much quicker than that of PCL crystals. Although the PEG crystals were nucleated later, they grew rapidly and surrounded the PCL spherulites immediately. Finally, the growth rate of the PEG crystals within the interlamellar regions of the inner PCL spherulites was much quicker than that out of the PCL spherulites. Therefore, the PEG crystals could grow out from the inner PCL spherulites and further induce the growth of the outer PEG spherulites from the front of the inner PCL spherulites, resulting in the formation of the concentric spherulites.

Conclusions

The diblock copolymer PEG_{50}−PCL_{50} exhibited a superposed crystallization temperature at 35.4 °C and a superposed melting point at 58.5 °C in the DSC curves recorded while scanning at 10 °C/min. However, the temperature-dependent FTIR measurements while cooling at 0.2 °C/min indicated that the PCL crystallized first from the copolymer melt. The PEG and PCL blocks of PEG_{50}−PCL_{50} formed the separate crystalline microdomains and constructed the alternating lamella regions of PEG and PCL.

During the isothermal crystallization of the copolymer, the PCL spherulites formed first, and the initial nucleation of the PEG crystals happened often within a PCL spherulite a certain time later. The PEG crystals grew quickly within the interlamellar regions of the PCL spherulite and then triggered the concentric growth of the outer PEG spherulite from the front of the PCL spherulite. The growth rate of the PEG crystals within the PCL spherulites was 15.1 μm/s, which was much quicker than that of the outer PEG spherulites, 4.4 μm/s. The reason was that the effective concentration of the molten PEG chains templated by the PCL crystalline lamellae was much higher than the average melt concentration. The PCL crystals within the interlamellar regions of the outer PEG spherulites also began to grow from the front of the inner PCL spherulites but did not change the total morphology of the outer PEG spherulites. The growth rate of the PCL crystals within the outer PEG spherulites was 0.15 μm/s, which was obviously slower than that of the inner PCL spherulites, 0.28 μm/s. The inner and outer portions of the concentric spherulites both contained the PCL and PEG crystals, but the morphology of the inner and outer portions was similar to that of the PCL and PEG spherulites, respectively. The PCL crystallinity of the inner portion of the concentric spherulites was a little higher than that of the outer portion, while the PEG crystallinity of the outer portion was a little higher than that of the inner portion, due to the confined crystallization of the PCL blocks restricted within the outer portion and the PEG blocks within the inner portion. Anyway, the contents of the PCL or PEG in the inner and outer portions of the concentric spherulites were the same.

Acknowledgment. This project is financially supported by the National Natural Science Foundation of China (project no. 20574066, 50373043), National Fund for Distinguished Young Scholar (no. 50425309) and Chinese Academy of Sciences (project no. KJCX2-SW-H07). The authors acknowledge Dr. Christian Burger in the Department of Chemistry, SUNY at Stony Brook, and Prof. Lisong Dong in CIAC for their helpful discussions.

References and Notes

(1) Masahiko, O. *Prog. Polym. Sci.* **2002**, *27*, 87.
(2) Kathryn, E. U.; Scott, M. C.; Robert, S. L.; Kevin, M. S. *Chem. Rev.* **1999**, *99*, 3181.
(3) Jeong, B. M.; Bae, Y. H.; Lee, D. S.; Kim, S. W. *Nature (London)* **1997**, *388*, 860.
(4) Chiellini, E.; Solaro, R. *Adv. Mater.* **1996**, *8*, 305.
(5) Robert, L. *Science* **1993**, *260*, 920.
(6) Lillie, E.; Schultz, R. C. *Macromol. Chem.* **1975**, *176*, 1901.
(7) Kricheldorf, H. R.; Berl, M.; Scharnagl, N. *Macromolecules* **1988**, *21*, 286.
(8) Nijenhuis, A. J.; Grijpma, D. W.; Pennings, A. J. *Macromolecules* **1992**, *25*, 6419.
(9) Albertsson, A. C.; Varma, K. *Biomacromolecules* **2003**, *4*, 1466.
(10) Piao, L. H.; Dai, Z. L.; Deng, M. X.; Chen, X. S.; Jing, X. B. *Polymer* **2003**, *44*, 2025.
(11) Tang, Z. H.; Chen, X. S.; Liang, Q. Z.; Bian, X. C.; Yang, L. X.; Piao, L. H.; Jing, X. B. *J Polym. Sci. Part A: Polym. Chem.* **2003**, *41*, 1934.
(12) Tang, Z. H.; Chen, X. S.; Pang, X.; Yang, Y.; Zhang, X.; Jing, X. B. *Biomacromolecules* **2004**, *5*, 965.
(13) Li, S.; Garreau, H.; Pauvert, B.; McGrath, J.; Toniolo, A.; Vert, M. *Biomacromolecules* **2002**, *3*, 525.
(14) Na, Y. H.; He, Y.; Shuai, X. T.; Kikkwa, Y.; Doi, Y.; Inoue, Y. *Biomacromolecules* **2002**, *3*, 1179.
(15) Kikkwa, Y.; Iwata, T.; Inoue, Y.; Doi, Y. *Biomacromolecules* **2002**, *3*, 350.
(16) Sun, J. R.; Hong, Z. K.; Yang, L. X.; Tang, Z. H.; Chen, X. S.; Jing, X. B. *Polymer* **2004**, *45*, 5969.
(17) Tsuji, H.; Tezuka, Y. *Biomacromolecules* **2004**, *5*, 1181.
(18) Tsuji, H.; Miyase, T.; Tezuka, Y.; Saha, S. K. *Biomacromolecules* **2005**, *6*, 244.
(19) Hamley, I. W.; Castelletto, V.; Castillo, R. V.; Muller, A. J.; Martin, C. M.; Pollet, E.; Dubois, P. *Macromolecules* **2005**, *38*, 463.
(20) Abe, H.; Harigaya, M.; Doi, Y. *Biomacromolecules* **2005**, *6*, 457.
(21) Yasin, M.; Tighe, B. J. *Biomaterials* **1992**, *13*, 9.
(22) Pitt, C. G. In *Biodegradable Polymers as Drug Delivery Systems*; Chasin, M., Langer, R., Eds.; M. Dekker: New York, 1990; p 71.
(23) Nojima, S.; Ono, M.; Ashida, T. *Polym. J.* **1992**, *24*, 1272.
(24) Gan, Z. H.; Jiang, B. Z.; Zhang, J. *J. Appl. Polym. Sci.* **1996**, *59*, 961
(25) Gan, Z. H.; Zhang, J.; Jiang, B. Z. *J. Appl. Polym. Sci.* **1997**, *63*, 1793.
(26) Bogdanov, B.; Vidts, A.; Van Den Bulcke, A.; Verbeeck, R.; Schacht, E. *Polymer* **1997**, *39*, 1631.
(27) Bogdanov, B.; Vidts, A.; Schacht, E. *Macromolecules* **1999**, *32*, 726.
(28) Shiomi, T.; Imai, K.; Takenaka, K.; Takeshita, H.; Hayashi, H.; Tezuka, Y. *Polymer* **2001**, *42*, 3233.
(29) Jiang, S. C.; He, C. L.; An, L. J.; Chen, X. S.; Jiang, B. Z. *Macromol. Chem. Phys.* **2004**, *205*, 2229.

(30) He, C. L.; Sun, J. R.; Deng, C.; Zhao, T.; Deng, M. X.; Chen, X. S.; Jing, X. B. *Biomacromolecules* **2004**, *5*, 2042.
(31) Wunderlich, B. *Macromolecular Physics, Crystal Nucleation, Growth, Annealing*; Academic Press: New York, 1976; Vol. 2, p 168.
(32) Chu, B.; Hsiao, B. S. *Chem. Rev.* **2001**, *101*, 1727.
(33) Yin, J. H.; Mo, Z. S. *Modern Polymer Physics*; Science Press: Bei Jing, 2001; p 947.
(34) Yin, J. H.; Mo, Z. S. *Modern Polymer Physics*; Science Press: Bei Jing, 2001; p 960.
(35) Mihailov, M.; Nedkov, E.; Goshev, I. *J. Macromol. Sci. Phys. B* **1978**, *15* (2), 313.
(36) Xue, M. L.; Sheng, J.; Yu, Y. L.; Chuah, H. H. *Eur. Polym. J.* **2004**, *40*, 811.

BM050627F